Study of N-benzoyl-L-argininate ethyl ester chloride, a model compound for poly(ester amide) precursors: X-ray diffraction, infrared and Raman spectroscopies, and quantum chemistry calculations

A. C. Fonseca, S. Jarmelo, M. Ramos Silva, A. M. Matos Beja, R. Fausto et al.

Citation: J. Chem. Phys. **134**, 124505 (2011); doi: 10.1063/1.3565966
View online: http://dx.doi.org/10.1063/1.3565966
View Table of Contents: http://jcp.aip.org/resource/1/JCPSA6/v134/i12
Published by the American Institute of Physics.

Study of N_α-benzoyl-L-argininate ethyl ester chloride, a model compound for poly(ester amide) precursors: X-ray diffraction, infrared and Raman spectroscopies, and quantum chemistry calculations

A. C. Fonseca,[1] S. Jarmelo,[1,2] M. Ramos Silva,[3] A. M. Matos Beja,[3] R. Fausto,[2] M. H. Gil,[1] and P. N. Simões[1,a)]
[1]*Department of Chemical Engineering, University of Coimbra, Pólo II, Pinhal de Marrocos, Coimbra 3030-790, Portugal*
[2]*Department of Chemistry, University of Coimbra, Coimbra 3004-535, Portugal*
[3]*Department of Physics, University of Coimbra, Coimbra 3004-536, Portugal*

(Received 20 December 2010; accepted 18 February 2011; published online 24 March 2011)

Poly(ester amide)s (PEAs) are lacking in structural and spectroscopic information. This paper reports a structural and spectroscopic characterization of N_α-benzoyl-L-argininate ethyl ester chloride ($BAEEH^+ \cdot Cl^-$), an important amino acid derivative and an adequate PEAs' model compound. Crystals of $BAEEH^+ \cdot Cl^-$ obtained by slow evaporation in an ethanol/water mixture were studied by different complementary techniques. X-ray analysis shows that $BAEEH^+ \cdot Cl^-$ crystallizes in the chiral space group $P2_1$. There are two symmetry independent cations (and anions) in the unit cell. The two cations have different conformations: in one of them, the angle between the least-squares planes of the phenyl ring and the guanidyl group is 5.1(2)°, and in the other the corresponding angle is 13.3(2)°. There is an extensive network of H-bonds that assembles the ions in layers parallel to the *ab* plane. Experimental FT-IR and Raman spectra of $BAEEH^+ \cdot Cl^-$ were recorded at room temperature in the 3750–600 cm^{-1} and 3380–100 cm^{-1} regions, respectively, and fully assigned. Both structural and spectroscopic analysis were supported by quantum chemistry calculations based on different models (*in vacuo* and solid-state DFT simulations). © *2011 American Institute of Physics*. [doi:10.1063/1.3565966]

I. INTRODUCTION

Poly(ester amide)s (PEAs), containing both ester and amide linkages in their structure, have been considered an important group of polymers in biomedical/pharmaceutical field. These materials combine in the same entity the better characteristics of polyamides (enhanced thermal and mechanical properties due to the establishment of strong H-bonds between the amide groups) and polyesters (high degradability).[1,2] Those composed by α-hydroxy acids and α-amino acids (commonly named polydepsipetides) are very popular.[3] The presence of α-amino acids in the structure of PEAs opens the possibility of degradation of these materials under enzymatic conditions, thus increasing their biodegradability.[4]

Although being materials of outstanding importance, there is a lack of information on the structural and spectroscopic properties of PEAs, probably due to the complexity of their long repeating unit.[1,5] Studies performed on PEAs derived from glycine, diols, and dicarboxylic acids revealed that their structural characteristics are a mix of those of polyamides and polyesters, showing the ability of establishing intermolecular H-bonds along a single direction.[1,6]

Because of the reasons mentioned here for the scarcity of structural and spectroscopic data on PEAs, it seems to be essential to perform studies on model compounds in order to get new insights about more complex systems. The model compound considered in this investigation is N_α-benzoyl-L-argininate ethyl ester chloride ($BAEEH^+ \cdot Cl^-$; Scheme 1).

$BAEEH^+ \cdot Cl^-$ was studied recently in gas phase and in solution.[7] The condensed (solid) state of $BAEEH^+ \cdot Cl^-$ was chosen as subject of the present study. This was targeted at new structural and spectroscopic data, assessed both experimentally and theoretically. The experimental work was accomplished by means of x-ray analysis and vibrational (IR and Raman) spectroscopy, whereas the theoretical approach was based on molecular modeling and simulation.

Quantum chemical calculations are a fundamental support in the assignment of spectroscopic data. However, in order to be reliable in such assignments when dealing with

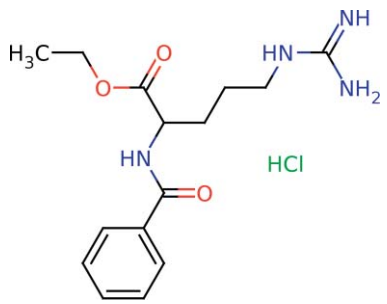

SCHEME 1.

a)Author to whom correspondence should be addressed. Electronic mail: pnsim@eq.uc.pt.

solid state data, there are some issues that should be tackled. Considering the $N = 46$ atoms in each $BAEEH^+ \cdot Cl^-$ entity and Z molecules present in the unit cell, a total of $138 \times Z$–3 normal vibrational modes [i.e., $(3 \times 46–6) \times Z = 528$ internal and $6 \times Z–3 = 21$ external modes] are expected. This raises the question of knowing wheather the calculated vibrational spectrum for the isolated $BAEEH^+$ cation *in vacuo* is sufficient to the normal mode assignments. In fact, the observed frequencies are perturbed by a crystalline force field, which is not accounted in the isolated-molecule calculations (not to mention the effects of neglecting anharmonicity). The same applies to specific kind of interactions within the crystal, the intermolecular H-bonding interactions being a notable example. It is of interest to integrate these topics with structural data.

As far as x-ray diffraction analysis is concerned, the uncertainty in locating the hydrogen atom positions and/or the difficulty in solving crystal structures exhibiting local disorders are well known problems. The resort to quantum chemical calculations is also a possible strategy toward the necessary corrections,[8] but the reliability of this approach depends on the quality of the theoretical model. Again, the results of calculations performed on an isolated molecule *in vacuo* must be cautiously taken if important environmental interactions actually exist within the crystal, such as H-bonding, torsions, and/or other crystal packing effects. Furthermore, in virtue of the different environments experienced by a molecule *in vacuo* and in the crystal, their possible conformations, and thus their minimum energy geometries, can contrast each other to a greater or lesser extent.

In order to evaluate the pertinence of these issues when applied to the title compound, the theoretical approach was extended to calculations based on a $BAEEH^+(H_2O)_5$ supermolecular structure and a solid-state model under periodic boundary conditions (PBC). The calculated data, integrated with and complementary to the experimental data, has provided a comprehensive structural and spectroscopic characterization of crystalline $BAEEH^+ \cdot Cl^-$.

II. MATERIALS AND METHODS

A. Experimental details

N_α-benzoyl-L-argininate ethyl ester chloride ($BAEEH^+ \cdot Cl^-$; purity $\geq$ 99.0%) was purchased from Fluka. Crystals of $BAEEH^+ \cdot Cl^-$ were obtained by slow evaporation of the solvent from a solution of $BAEEH^+ \cdot Cl^-$ (7 mM) in an ethanol/water mixture (50:50, V/V), at room temperature.

X-ray data were collected on a Bruker APEX II-CCD diffractometer, using a colorless block-shaped crystal with dimensions 0.15 × 0.13 × 0.08 mm. The crystallographic structure was solved by direct methods using SHELXS-97. Refinements were carried out with the SHELXL-97 package.[9] All refinements were made by full-matrix least-squares on F^2. Anisotropic displacement parameters were used for all nonhydrogen atoms with exception of those in the terminal ethyl group. In both molecules, the ethyl group is disordered over two positions with 40/60 refined occupancies. Hydrogen atoms were refined using a riding model. X-ray data confirmed the expected stereochemistry; the Flack parameter refined down to 0.07(9).[10] The fractional atomic coordinates and equivalent isotropic displacement parameters and other supplementary data have been deposited at the Cambridge Crystallographic Data Center (CCDC 796634).

The room-temperature IR spectrum (3750–600 cm^{-1}) of solid polycrystalline $BAEEH^+ \cdot Cl^-$ in a KBr pellet was obtained using a Bomem (MB104) Fourier transform spectrometer equipped with a deuterated triglycine sulphide detector and Zn/Se optics. Data collection was performed with 4 cm^{-1} spectral resolution and 128 scans.

The room-temperature Raman spectrum (3380–100 cm^{-1}) of solid polycrystalline $BAEEH^+ \cdot Cl^-$ pressed in a pellet (neat solid) was obtained using a dispersive Raman instrument, model DXR SmartRamanTM spectrometer from Thermo Fisher Scientific Inc., equipped with a low-power, externally stabilized diode laser, 780 nm wavelength, with a power at output of laser head of 13 mW. The calibration of the instrument is performed once weekly with the patented autoalignment and automated calibration device. Data collection was performed with an exposure time to laser radiation of 15 s, 10 sample exposures and a slit aperture of 25 μm. Fluorescence correction was performed using a polynomial of fifth degree.

B. Computational details

The theoretical study was accomplished by using three models: (i) an isolated $BAEEH^+$ molecule *in vacuo* (for simplicity hereafter referred as model M.I); (ii) a $BAEEH^+(H_2O)_5$ complex *in vacuo* (model M.II) to simulate H-bonding interactions; (iii) a solid-state model (model M.III) under Periodic Boundary Conditions (PBC), to account for other possible packing effects not predicted by the above referred models *in vacuo*. These theoretical models were established from the crystallographic data obtained in the present study (see Fig. 1).

The calculations *in vacuo* were performed with the GAUSSIAN03 package[11] at the density functional theory (DFT) (Ref. 12) level of approximation, using the Becke style 3-parameter with the Lee–Yang–Parr correlation functional (B3LYP) (Refs. 13 and 14), and the 6-31++G(d,p) (Ref. 11) Pople-type basis set. For each model, the molecular geometries were fully optimized by the force gradient method using the Berny algorithm.[15] In all cases, the nature of the stationary points was confirmed by vibrational frequency calculations. The B3LYP/6-31++G(d,p) wavenumbers reported in this study were scaled by a factor of 0.965.

The $BAEEH^+ \cdot Cl^-$ crystalline phase was investigated theoretically within a plane-wave-based DFT framework under PBC. For this purpose, the Car-Parrinello Molecular Dymamics (CPMD) code[16] with Goedecker-type pseudopotentials[17] and the BLYP exchange-correlation functional[13] were used. The initial structures were taken from the x-ray diffraction data. Different plane-wave cutoffs were tested for checking convergence. The CPMD results presented henceforth correspond to a plane-wave cutoff of 160 Ry and

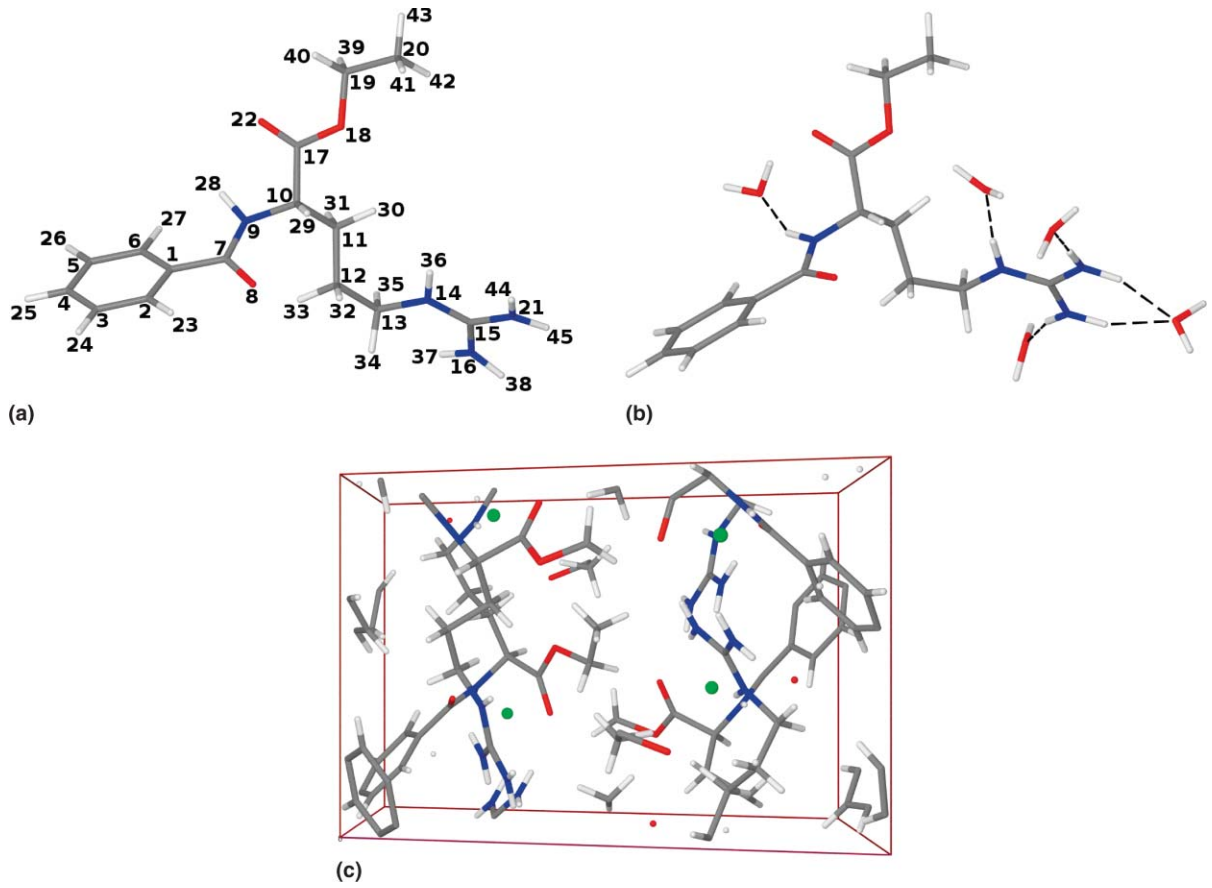

FIG. 1. Different theoretical models used in the simulation of the structural and spectroscopic properties of N_{α}-Benzoyl-L-Argininate Ethyl Ester Chloride ($BAEEH^{+} \cdot Cl^{-}$): (a) B3LYP/6-31++G(d,p) calculations of isolated $BAEEH^{+}$ *in vacuo*, (b) B3LYP/6-31++G(d,p) calculations of a $BAEEH^{+}(H_2O)_5$ complex *in vacuo*, and (c) CPMD calculations under periodic boundary conditions of a $BAEEH^{+} \cdot Cl^{-}$ crystal. The three theoretical models were established from the x-ray crystallographic data.

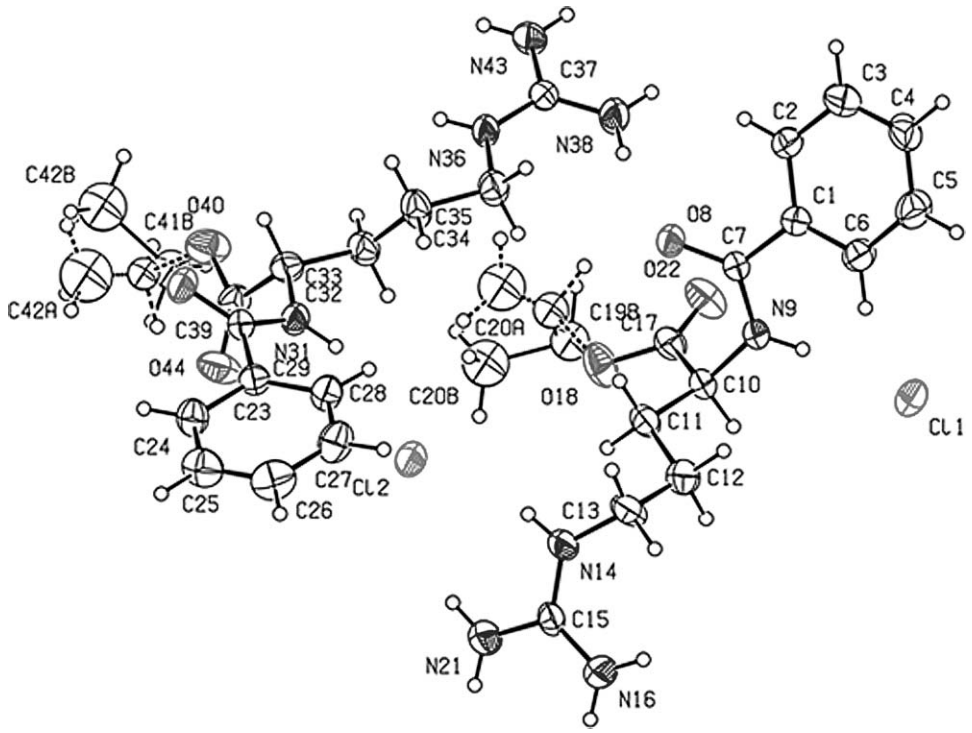

FIG. 2. ORTEP diagram of $BAEEH^{+} \cdot Cl^{-}$. The ellipsoids were drawn at the 30% probability level for clarity reasons. The alternative conformations of the ethyl groups are shown. Black and dashed lines are used for the minor and major components, respectively.

TABLE I. X-ray and calculated (PBC geometry optimization) data on the hydrogen-bonding related geometric parameters in the crystal of $BAEEH^+ \cdot Cl^-$ (D: donor; A: acceptor). See Fig. 2 for atom numbering.

	D−H (Å)		H · · · A (Å)		D · · · A (Å)		D−H · · · A (°)	
D−H · · · A	Exp	Calc	Exp	Calc	Exp	Calc	Exp	Calc
INTERMOLECULAR								
AMIDE MOIETY								
$N-H_{(Amide\ 1)} \cdots Cl_{(1)}$	0.86	1.029	2.34	2.121	3.094(4)	3.093	146	156.7
$N-H_{(Amide\ 2)} \cdots Cl_{(2)}$	0.86	1.030	2.49	2.261	3.253(5)	3.268	148	165.5
GUANIDYL MOIETY								
N−H GROUPS								
$N-H_{(1)} \cdots Cl_{(2)}$	0.86	1.031	2.35	2.183	3.186(5)	3.195	164	166.7
$N-H_{(2)} \cdots Cl_{(1)}$	0.86	1.029	2.45	2.200	3.195(5)	3.183	145	159.3
NH_2 GROUPS								
$N-H_{(16A)} \cdots Cl_{(1)}$	0.86	1.022	2.57	2.390	3.351(5)	3.335	151	153.3
$N-H_{(16B)} \cdots O=_{(Amide\ 2)}$	0.86	1.023	1.98	1.837	2.809(6)	2.845	161	167.6
$N-H_{(38A)} \cdots Cl_{(2)}$	0.86	1.028	2.37	2.202	3.203(4)	3.220	163	170.2
$N-H_{(38B)} \cdots O=_{(Amide\ 1)}$	0.86	1.023	2.05	1.860	2.890(6)	2.876	166	171.2
$N-H_{(21A)} \cdots O=_{(Ester\ 1)}$	0.86	1.023	2.08	1.845	2.800(7)	2.799	141	153.6
$N-H_{(21B)} \cdots Cl_{(2)}$	0.86	1.018	2.61	2.480	3.378(5)	3.407	150	151.1
$N-H_{(43A)} \cdots O=_{(Ester\ 2)}$	0.86	1.014	2.40	2.199	2.914(6)	2.838	119	119.3
$N-H_{(43B)} \cdots Cl_{(1)}$	0.86	1.019	2.54	2.374	3.281(5)	3.286	145	148.4
INTRAMOLECULAR								
$C-H_{(Para\ 1)} \cdots O=_{(Amide\ 1)}$	0.93	1.084	2.57	2.448	3.371(7)	3.390	144	144.5
$C_{(11)}-H \cdots O_{(Ester\ 1)}$	0.97	1.091	2.38	2.409	2.717(8)	2.753	100	96.4
$C_{(13)}-H \cdots N_{(16\ Amine\ 1)}$	0.97	1.091	2.57	2.663	2.905(7)	2.962	100	94.8
$C_{(41)}-H \cdots O=_{(Ester\ 2)}$	0.97	1.090	2.29	2.339	2.671(10)	2.755	102	100.5
$C_{(34)}-H \cdots N-H_{(2)}$	0.97	1.096	2.62	2.710	2.962(8)	2.463	101	65.3

convergence criteria for geometry optimizations of 5×10^{-4} atomic units. An average position of the ethyl group (which exhibits a disordered over two positions; see below) was considered for calculation purposes.

III. RESULTS AND DISCUSSION

A. X-ray crystallography

Figure 2 shows the ORTEP diagram of $BAEEH^+ \cdot Cl^-$ determined by x-ray diffraction. Table I summarizes the three-dimensional hydrogen bonding network crystallographic parameters of the title compound.

The $BAEEH^+ \cdot Cl^-$ crystal was found to be monoclinic (space group: $P2_1$), with four molecules in the unit cell (two of them are symmetry-independent), whose volume is 1851.7(2) $Å^3$ and lattice constants are as follows: $a = 11.9236(8)$, $b = 10.3583(6)$, and $c = 15.8540(10)$ Å, and $\beta = 108.976(4)^\circ$, at ambient conditions. As expected, the imine (=N−H) group of the guanidyl moiety is protonated in both cations, as shown by the C−N distances of $–NH_2$ amine groups: 1.305(4) Å for C15−N16, 1.332(4) Å for C15−N21, 1.314(4) Å for C37−N38, and 1.315(4) Å for C37−N43 (see Fig. 2 for atom labeling). The symmetry independent cations show different conformations. In one cation the C15-N14-C13-C12 torsion angle is 172.4(3)° while in the other is 101.3(4)°, here labeled as cations A and B, respectively (see Fig. 2 for atom labeling). The angle between the least-squares planes of the phenyl ring and the planar guanidyl group is 5.1(2)° for A and 13.3(2)° for B. Both cations display unambiguous S configurations at their chiral centres (C10 and C32). The ethyl group of both molecules is disordered over two sites (see Fig. 2).

There is an extensive network of H-bonds that exhausts the cations donor capacity (Fig. 3). The H-bonds assemble the ions in layers parallel to the *ab* plane (Fig. 4). The experimental x-ray data suggests that weak intramolecular H-bonds may also be formed in $BAEEH^+ \cdot Cl^-$, as it can be checked in Table I. The results summarized in Table I also show that the CH and NH bond lengths computed from the solid-state model are substantially longer than the values given by the x-ray analysis (a similar trend was obtained by the other models; see below). This discrepancy is an expected result of the uncertainty in locating the hydrogen atoms by x-ray diffraction, as well as a consequence of the riding model used in the structural refinement.

The two symmetry independent cations (A and B) previously described are thus under the influence of two quite strong types of crystal packing factors, i.e., intermolecular H-bonds and ionic interactions. In fact, both solid state conformers were taken into account in the theoretical calculations as input geometries for the isolated-molecule optimizations performed *in vacuo*, and both structures exhibited noticeable changes along the geometry optimization. The most dramatic difference occurred in cation B [see Fig. S1 in the SI (Ref. 18); prefix "S" in the names of figures and tables stands for supplementary material] whose

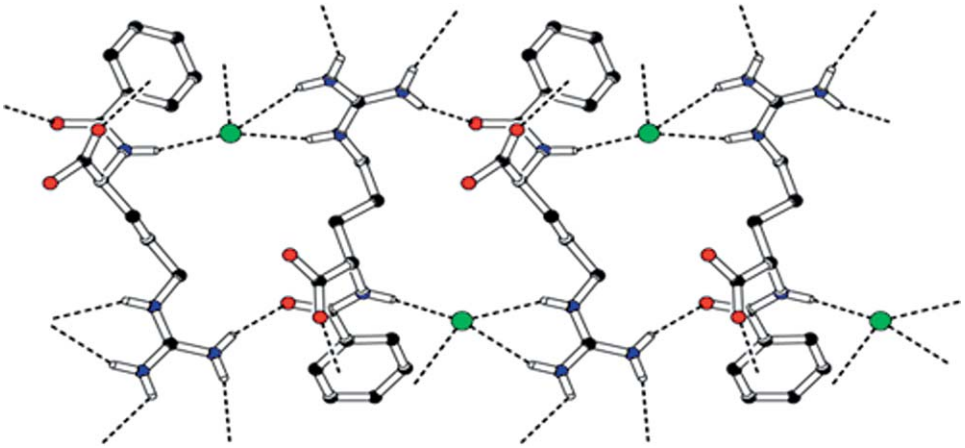

FIG. 3. H-bond network of $BAEEH^+ \cdot Cl^-$ determined by x-ray diffraction. Disordered atoms and H atoms not involved in H-bonding were omitted for clarity reasons.

optimized structure was found to be ~19 kJ mol^{-1} more stable (total energies corrected by zero-point energy) than cation A. The increased stability of the calculated structure resulting from cation B is mainly due to an intramolecular bifurcated H-bond established between the carbonyl oxygen atom of amide linkage and the guanidyl group [$N-H_{Imine} \cdots O_{Carbonyl}$: $d(H_{Imine} \cdots O_{Carbonyl}) = 1.813$ Å, $\angle(N-H_{Imine} \cdots O_{Carbonyl}) = 150.3^o$; $N-H_{Amine} \cdots O_{Carbonyl}$: $d(H_{Amine} \cdots O_{Carbonyl}) = 2.110$ Å, $\angle(N-H_{Amine} \cdots O_{Carbonyl}) = 139.7^o$]. On the other hand, the structure resulting from the optimization of cation A appears to be stabilized just by some bond torsions, namely by adopting a conformation in which the aromatic ring is twisted by ~60° relative to the starting structure present in the crystal [see Fig. S1 (Ref. 18)]. The angle between the least-squares planes of the aromatic ring and the guanidine moiety changed from 13° to 72° in the course of optimization. Apart from this main feature, the optimized structure for A is much more comparable to the solid state conformations. Consequently, the data derived from calculations performed *in vacuo* are referred only to cation A. The aforementioned model M.I corresponds then to the optimized (*in vacuo*) cation A, from which the model M.II was established through a further optimization (also *in vacuo*) of the $BAEEH^+(H_2O)_5$ complex. Thus, in what follows, the comparisons between experimental (x-ray analysis) and calculated data are referred to models M.I, M.II, and M.III as far as cation A is concerned, and only to model M.III in the case of cation B.

Figure 5 compares graphically the structural data obtained experimentally and computationally, the later based on the three theoretical models referred above. The main features related with covalent bonds can be summarized as follow [see Fig. S2 in the SI (Ref. 18) for geometrical parameters involving hydrogen atoms, Figs. S3 and S4 for similar data referred to cation B, and Table S1 for root mean square deviation (RMSD) and maximum/minimum deviations from experiment]: (i) the results can be clustered into two groups, which are related with the participation or not of a hydrogen atom in the bond; (ii) most of the calculated bonds are predicted to be longer than the experimental ones; (iii) the trends underlying items (i) and (ii) are consistently predicted by the three theoretical models here considered; (iv) these global patterns are commonly applicable to both conformers, A and B.

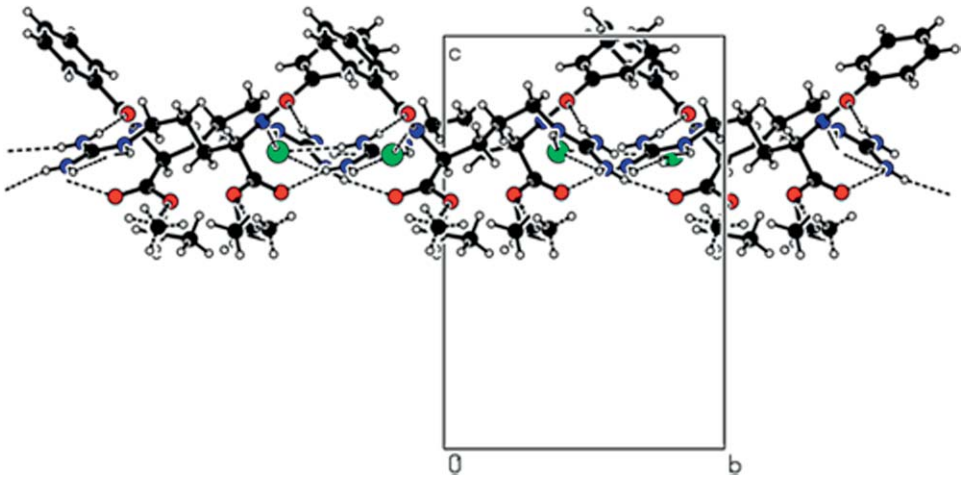

FIG. 4. One layer of bonded ions through H-bonds.

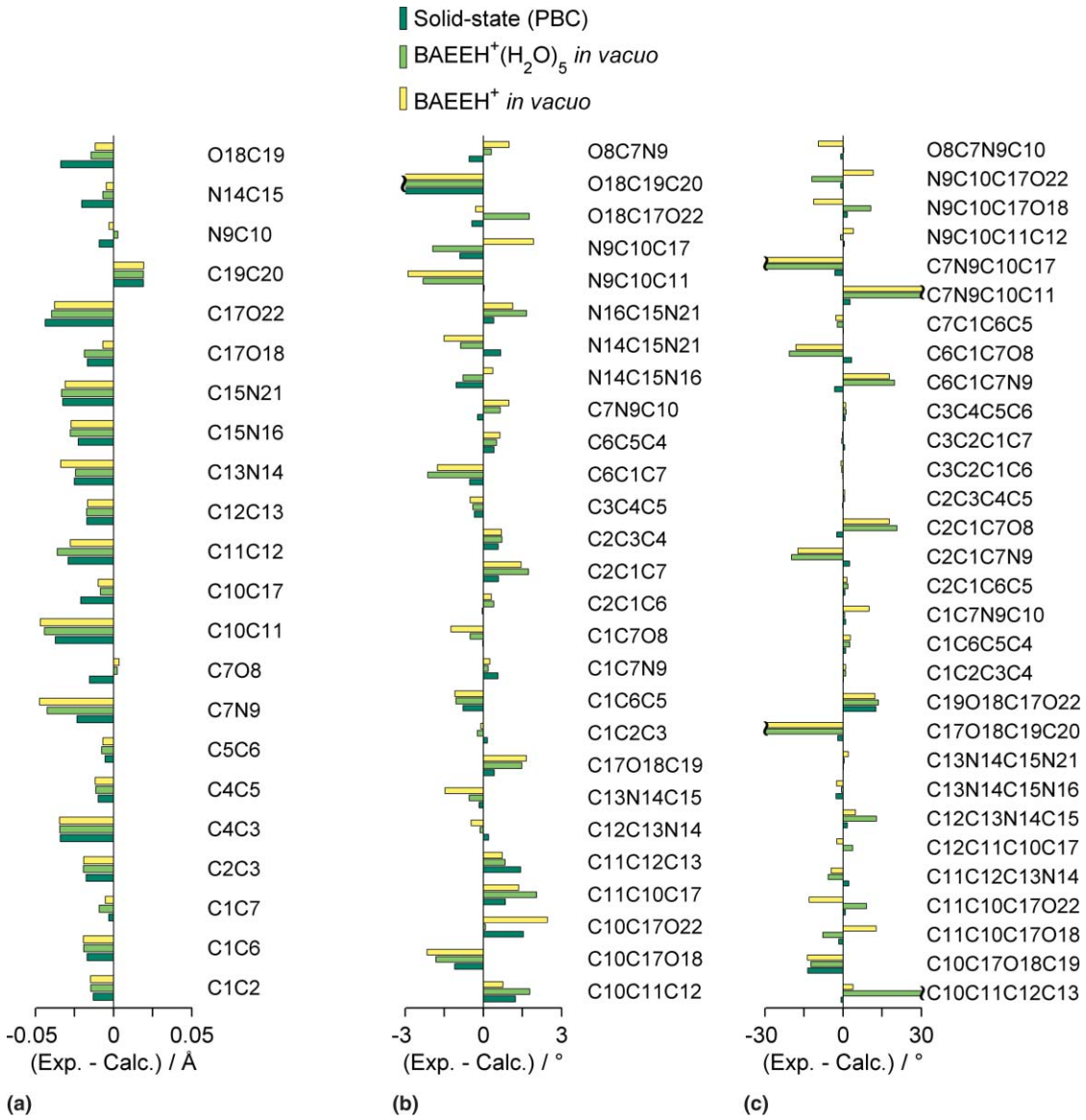

FIG. 5. (a) Bond length, (b) valence angle, and (c) torsion angle differences between experimental (x ray) and computed data from different models for conformer **A** (case referred to geometrical parameters not involving hydrogen atoms; see Fig. 2 for atom labeling).

As anticipated, the computed CH and NH bond lengths are substantially longer than the experimental values. The maximum deviation from experiment of 0.170 Å is predicted by the solid-state model in the case of NH imine bond for both conformers A and B. In terms of RMSD values, these are within a small range (from 0.140 to 0.143 Å) considering all theoretical models under comparison [see Table S1 in the SI (Ref. 18)]. These results are in clear contrast with those for bonds involving only heavy atoms, whose bond length differences from experimental data are much less pronounced (one order of magnitude less). The worst predictions correspond to a difference of 0.047 Å for the C7N9 bond in conformer A, obtained from model M.I, and of 0.054 for the C10C17 bond in conformer B, computed from model M.III [see Table S1 in the SI (Ref. 18)]. The RMSD value of 0.024 Å across all models found in the case of conformer A appeared to be slightly worsened in the conformer B (RMSD of 0.028 Å).

It is worth mentioning the remarkable agreement between the results obtained from solid-state model and those from the models whose computations were performed *in vacuo*. This shows that the incorporation of environmental interactions in the model does not significantly changes the computed bond lengths. The observed consistency across the models and its quite acceptable performance in describing the experimental bond lengths between heavy atoms should also be highlighted.

In the case of valence angles, whether involving hydrogen atoms or not, the RMSD and maximum deviation from experimental are comparable among the three models [see Fig. 5 and Table S1 in the SI (Ref. 18)]. Again, the agreement between calculated and experimental data is within relatively narrow limits, with a maximum deviation of 7.2° for the O18C19C20 angle in conformer A, predicted from model M.III (it should be reminded that an average position over the two sites of the ethyl group found in the x-ray analysis was

considered) and a RMSD of only 1.8° as the worst case. The performance of model M.III in the case of cation B is similar to that for cation A. The models performed *in vacuo* are as accurate as its solid-state counterpart in bond angle predictions, which is a noticeable result taking into account the different conformation adopted by the isolated $BAEEH^+$ or its water complex after the respective optimizations *in vacuo*.

As it can be seen from Fig. 5 [see also Table S1 in the SI (Ref. 18)], the most representative discrepancies between experimental and calculated torsion angles are the dihedrals C7N9C10C17 (maximum deviation of 62° predicted by model M.I), C7N9C10C11 (maximum deviation of ~39° predicted by model M.II), C17O18C19C20 (deviation of ~36° predicted by both models M.I and M.II), C10C11C12C13 (deviation of ~31° predicted by M.II). These extreme deviations are mostly responsible for the relatively high RMSD values of 19.5° and 16.1°, respectively for models M.I and M.II, when compared to only 3.8° (3.0° for cation B) for the solid-state model M.III. A similar trend is observed for torsions involving hydrogen atom(s), although in this case some of the major departures from experimental data appeared to be ascribable to the influence of the water molecules on isolated molecule calculations [see Fig. S2 in the SI (Ref. 18)]. Apart from the mentioned utmost deviations, the performance of the three models is quite similar, allowing fairly reasonable predictions to be achieved.

This structural analysis has revealed that for the system under study the resort to the solid-state scheme (model M.III) provides only a marginal enhancement in predicting bond lengths and valence angles. Torsion angles are the geometrical parameter which better reflects the stabilizing attributes of the crystal packing organization with respect to molecular conformers. Not surprisingly, the largest deviations from experimental values were justly observed for dihedral angles, revealing in this way the effect of the optimizations performed *in vacuo*. Despite this relevant feature, globally the models M.I and/or M.II appeared to be a good alternative to the solid state-model, with the advantage of being considerably less demanding (mainly the simplest model) in terms of computational resources. For other theoretical issues analyzed in this study, such as the influence of the basis set (double versus triple zeta Gaussian type basis sets) or the DFT functional (generalized gradient approximation BLYP versus hybrid B3LYP functionals),[19] see Table S2 in the SI (Ref. 18).

To conclude this analysis, it appeared that the favorable attributes and the great potential of the solid-state models under PBC in describing crystalline solids were made less evident in the particular system here studied. The theoretical investigation with the less demanding model M.I or even the model M.II accomplished with the B3LYP/6-31++G(d,p) was shown to be a good compromise.

B. Infrared and Raman spectra of $BAEEH^+ \cdot Cl^-$ crystal (room temperature)

Figure 6 shows the experimental FT-IR and Raman spectra of solid BAEEH+ · Cl− recorded at room temperature. Also presented in Fig. 6 are the B3LYP/6-31++G(d,p) simulated IR and Raman spectra of models M.I and M.II.

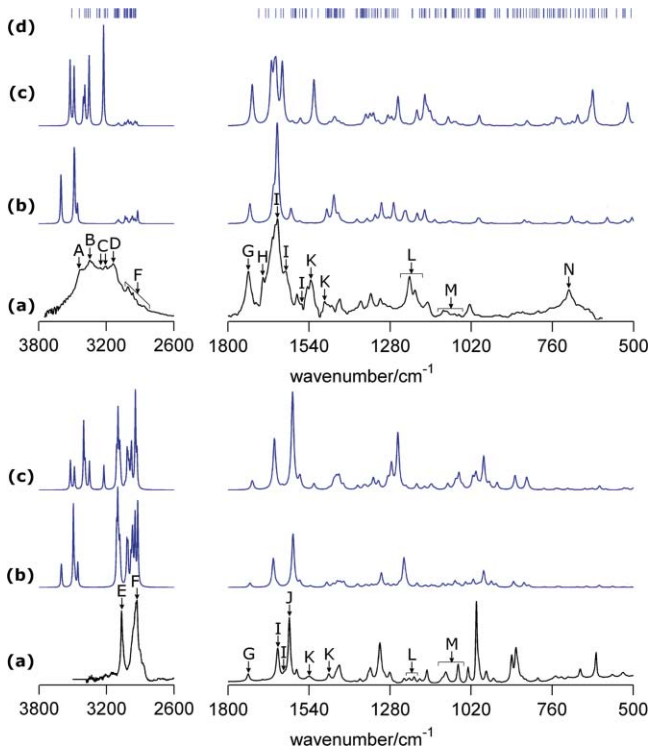

FIG. 6. FT-IR (top) and Raman (bottom) experimental spectra of solid $BAEEH^+ \cdot Cl^-$ recorded at room temperature (a); B3LYP/6-31++G(d,p) simulated spectra *in vacuo* of $BAEEH^+$ (b) and $BAEEH^+(H_2O)_5$ complex (c) (calculated wavenumbers were scaled by a factor of 0.965; bands due to water were excluded for clarity); and vibrational frequencies from the solid-state model (d) (intensities are not provided by the CPMD code). The features indicated by arrows correspond to the following: A: $(\nu NH_2\ as.)_{Guan}$; B: νNH_{Guan}; C: $(\nu NH_2\ s.)_{Guan}$; D: νNH_{Amide}; E: νCH_{Ring}; F: νCH; G: $\nu C{=}O_{Ester}$; H: $\nu C{=}O_{Amide}$; I: δNH_{Guan}; J: $\nu C{-}C_{Ring}$; K: δNH_{Amide}, $\nu C{-}N_{Amide}$; L: $\nu C{-}O{-}C_{Ester}$ as.; M: ρNH_{Guan}; N: ρCH_{Ring}.

Figure 6 includes also the frequencies computed from CPMD code (which does not provide intensities).

A first look to the results shown in Fig. 6 suggests a quite reasonable agreement between the experimental and the calculated spectroscopic data, with the exception of the band broadness actually observed in the NH stretching region in the IR spectrum. A closer analysis confirmed the general competency of the theoretical approach, being interesting to notice the fairly good performance achieved by the simplest model here used (model M.I) in predicting most of the experimental spectral features, and thus its usefulness in supporting most of the spectral assignments. There are some foreknown exceptions, such as its inadequacy to accurately reproduce experimental intensities, as well as its lacking in describing the red/blue shifts of stretching/bending modes due to moieties participating in H-bond interactions. The latter deficiency appears somewhat mitigated in the case of model M.II, which, although in a simplified way, accounts for such type of interactions. The influence of the water H-bonds (model M.II) has led to the interchange of the order of frequencies of some vibrational modes, whereas most of skeleton modes and those related with moieties not involved in intermolecular interactions appeared at quite similar frequencies in both M.I and M.II models.

The simulated spectra from the M.I or M.II models are much easier to interpret when compared with the outcome of the solid-state calculations based on model M.III. The latter is rather complicated by the Davydov splitting (factor-group splitting) of the vibrational modes according to the $Z = 4$ crystal cell, and at the same time by a considerable mixing of some modes in certain wavenumber ranges. On the other hand, the inability of the CPMD code to calculate IR intensities precludes every potential of model M.III to be fully explored within this context. Despite such drawback, the results of the solid-state calculations have shown to be a valuable complementary approach, which gathered with the calculated spectra from models M.I or M.II gives consistency to the IR spectroscopic analysis of the title compound.

Crossing the data from both experimental and computed sources, together with the support of reported vibrational spectra of similar compounds (in particular of the most characteristic vibrational bands of the guanidinium, carboxylic ester, amide, and benzene moieties), made possible plausible vibrational attributions to be done. Table II summarizes some representative experimental vibrational modes of $BAEEH^+ \cdot Cl^-$ and respective assignments. Table S3 in the SI (Ref. 18) includes the B3LYP/6-31++G(d,p) calculated IR and Raman spectra for the isolated-$BAEEH^+$ (the B3LYP vibrational spectra for model M.I was further simulated using the 6-311++G(d,p) basis set; the obtained results, which are also presented in Table S3 in the SI (Ref. 18), are comparable to those provided by the double-zeta basis set).

Table S4 in the SI (Ref. 18) shows B3LYP/6-31++G(d,p) calculated IR and Raman spectra of $BAEEH^+(H_2O)_5$ complex *in vacuo* (model M.II). A comparison between selected IR data from the models M.I, M.II, and M.III is presented in Table S5 [in the SI (Ref. 18)].

Below a short discussion of the assignments made for the vibrations of the structurally most relevant groups in $BAEEH^+ \cdot Cl^-$, i.e., those participating in H-bond interactions in the crystal (guanidinium, carboxylic ethyl ester, and amide moieties) is presented. A detailed discussion of the spectral assignments of bands due to the remaining molecular fragments (phenyl group and carbon chain) is presented in SI (Ref. 18).

1. Guanidinium moiety, $-N^+H{=}C(NH_2)_2$

According to the x-ray data, the $-NH_2$ groups are involved in two major types of intermolecular H-bonds, one established with the carbonyl (ester and amide) oxygen atom, and the other with the counterion (Cl^-). Thus, the stretching and bending vibrations of these groups may be used to investigate the $N-H\cdots O_{Carbonyl(Ester/Amide)}$ and $N-H\cdots Cl^-$ hydrogen-bonds. The four expected νNH_2 stretching vibrations give rise to the IR bands at 3435 (νNH_2 asymmetric; band A in Fig. 6) and 3252/3202 cm^{-1} (νNH_2 symmetric; band C), the two νNH_2 as modes contributing to the single observed band assigned to this type of vibrations. The stretching vibration of the imine group, on the other hand, is assigned to the broad intense band, with main maximum at 3346 cm^{-1} (band B). The broad structured profile observed in the N–H stretching region of the spectrum is a well-known characteristic of the spectra of zwitterionic or cationic forms of amino acids[20] and a consequence of the H-bond interactions, as well as Fermi resonance interactions with low energy vibrations.

It would be of interest to compare the observed spectrum for $BAEEH^+ \cdot Cl^-$ in this spectral region with those of other compounds bearing guanidinium group, in the crystalline state, in order to obtain information on the H-bonding. The N–H stretching vibrations of guanidinium cations have been observed in spectra of guanidinium complexes in a wide range of wavenumbers. However, it can be stated that the guanidinium moiety in $BAEEH^+ \cdot Cl^-$ is involved in stronger H-bonds than those present in most of the previously studied guanidinium salts (for example, the N–H stretching vibrations in NO_3^-, ClO_4^-, BF_4^-, and I^- guanidinium salts were observed at 3682, 3601, 3600, and 3561 cm^{-1}, respectively[21]). On the other hand, a similar value was observed for the crystals of guanidinium hydrogenselenate (3449 cm^{-1}) (Ref. 22), hydrogenarsenate monohydrate (3441 cm^{-1}) (Ref. 23), and hydrogensulphate (3462 cm^{-1}) (Ref. 24).

The frequencies for NH_2 vibrational modes for the isolated molecule are predicted at 3603 and 3599 cm^{-1} (asymmetric modes), and at 3485 and 3480 cm^{-1} (symmetric), whereas the imine stretching mode is predicted at 3494 cm^{-1} with smaller IR intensity. The significant overestimation of the frequencies of these vibrational modes is an expected consequence of the weakness of the model M.I for not accounting for the actual intermolecular interactions existing in the crystal. As previously explained, this limitation was addressed by two different approaches. The calculations based on the model M.II significantly red-shifted the NH stretching modes [variable, depending on the geometries of the simulated H-bonds: 119 cm^{-1} for νNH_2 as., 78 cm^{-1} for $\nu NH'_2$ as, 274 cm^{-1} for νNH, 132 cm^{-1} for $\nu NH'_2$ s., and 77 cm^{-1} for νNH_2 s.; as. and s. represent antisymmetric and symmetric modes, respectively; see Tables S3 and S4 in the SI (Ref. 18)], thus predicting these modes within a spectral range more close to the experimental one [see Table S5 in the SI (Ref. 18)]. Being also red-shifted under the solid-state simulation (model M.III), the NH frequencies are, in addiction, predicted to be split over different ranges, depending on the specific mode. The splitting of the νNH_2 asymmetric mode occurs over the largest range of *ca.* 191 cm^{-1} (considering both conformers A and B), whereas the range for the νNH_{Imine} mode is more modest (40 cm^{-1}) [see Table S5 in the SI (Ref. 18)].

The deformation vibrations of the $-NH_2$ group should be observed in the region between 1650–1550 cm^{-1} (in-plane bending modes, δ) and in the region 1150–1100 cm^{-1} (rocking modes, ρ). Each $-NH_2$ group of guanidinium moiety also has a wagging (ω) and torsional (τ) mode, which are expected to lie below 800 cm^{-1}.[25]

Analysis of the normal modes calculated for $BAEEH^+$ (model M.I) has revealed that the NH_2 bending mode of the guanidinium moiety contributes to four vibrations, predicted to occur in the IR spectrum at 1643 cm^{-1} (1661 cm^{-1} by model M.II), 1640 cm^{-1} (1646 cm^{-1}), 1598 cm^{-1} (1627 cm^{-1}), and 1535 cm^{-1} (1566 cm^{-1}). The two higher

TABLE II. Observed IR data for $BAEEH^+ \cdot Cl^-$ (polycrystalline sample pressed in a KBr pellet). The observed Raman data for $BAEEH^+ \cdot Cl^-$ (pellet of neat polycrystalline sample) are presented in parentheses.

Wavenumbers (cm^{-1})	Approximate description
HIGH FREQUENCY SPECTRAL REGION	
3435;3346;3252;3202;3139	N–H GUANIDINE AND AMIDE GROUPS
(n.i.)	νNH
	C–H RING
3080[a]	
(3066)	νCH
	C–H ESTER/LINEAR CARBON CHAIN (LCC)
3008;2963;2937;2929;2900;2867	νCH
(n.o.;2964;2937;2930;2903;2870)	
LOW FREQUENCY SPECTRAL REGION	
1734;1711	$\nu C{=}O_{Ester}$
(1736)	
1688;1657;1649;1641;1617;1603;1579;1564	$\nu C{=}O_{Amide}$;$\delta NH_{2\ Guan}$;$\nu C{-}N_{Guan}$;νCC_{Ring}
(1689;n.o.;n.o.;1641;1621;1603;1580;n.o.)	
1545;1535;1515;1500;1491;1477;1468	δNH_{Amide};$\nu C{-}N_{Amide}$
(1540;1476)[b]	
1442	$\delta NH_{Guan\ (Imine)}$;$\nu C{-}N_{Guan}$
(1443)	
1435-1365[c]	$\delta CH_{Ester/LCC/Ring}$
1358; 1343;1311;1298	$\omega CH_{2Ester/LCC}$;δCH_{Ring}
(1360;1343;1312;1298)	
1300-1175[d]	$twCH_{2\ LCC}$;$\nu C{-}O{-}C_{Ester}$ as δCH_{Ring} ρCH_{LCC};$\rho CH_2/\rho CH_{3Ester}$
1175-1045[e]	$\rho NH_{2\ Guan}$;$\rho NH_{Guan\ (Imine)}$; ρNH_{Amide} $\rho CH_{2\ LCC}$;$\rho CH_2/\rho CH_{3Ester}$ δCH_{Ring}
1045-865[f]	ρCH_{Ring};$\nu C{-}C_{Ester}/_{LCC}$
855;843	$\nu C{-}O{-}C_{Ester}$ s
(855;846)	
830-720[g]	$\rho CH_{Ring;}\rho C{=}O_{Amide}$
720;708;695	ρCH_{Ring}(all-in-phase);ρNH_{Amide}
(n.o.;710;707;698;688) 685-600[h]	ρCH_{Ring};$\rho C{=}O_{Ester}$;$\rho CN_{3\ Guan}$;$\delta O{=}C{-}N$;$\delta C{-}C{-}C_{Ring}$
n.i.	δN(16)–C–N(21);$\tau NH_{2\ Guan}$
(567)	
n.i.	$\rho C(11)H_2$;δN_{Amide}–C(10)–C(11)
(532)	
n.i.	δN(14)–C–N(21)
(493)	
n.i.	$\tau C{-}C_{Ring}$
(427;404)	
n.i.	$\delta C{-}O{-}CH_{2\ Ester}$
(373)	
n.i.	δC(17)–C(10)–N_{Amide};ωNH_2
(337)	
n.i.	τC(12)–C(13)
(313)	
n.i.	$\tau CH_2{-}CH_{3\ Ester}$

TABLE II. (*Continued*)

Wavenumbers (cm^{-1})	Approximate description
LOW FREQUENCY SPECTRAL REGION	
(253)	
n.i.	Vibration of Guanidyl (n.a.)
(194)	
n.i.	Vibration of Benzene (n.a.)
(180)	
n.i.	τC(11)–C(12)
(137)	

[a]It appears as a shoulder, which is overlapped by the NH stretching vibrations.
[b]The IR bands at 1545, 1535, and 1515 cm^{-1} give rise to a single Raman band at 1540 cm^{-1} and the IR bands at 1500, 1491, 1477, and 1468 cm^{-1} give rise to a single Raman band at 1476 cm^{-1}.
[c]In this wavenumbers range, the most intense IR band is located at 1374 cm^{-1} and it has a correspondence in the Raman spectrum at 1376 cm^{-1}, which is also the most intense band in the wavenumbers range under discussion.
[d]In the 1300–1175 cm^{-1} range, four bands (1281, 1218, 1200, and 1185 cm^{-1}) are observed in the IR spectrum. In the Raman spectrum, in the same spectral range, five bands (1281, 1235, 1218, 1202, and 1185 cm^{-1}) are observed. The IR bands at 1218 and 1200 cm^{-1} and the correspondent Raman bands at 1220 and 1203 cm^{-1} are assigned to the νC–O–C_{Ester} as vibrations.
[e]In the 1175–1045 cm^{-1} range, five bands are observed (IR: 1160, 1109, 1099, 1074, and 1061 cm^{-1}; Raman: 1162, 1109, 1100, and 1062 cm^{-1}).
[f]In the 1045–865 cm^{-1} range several bands in the IR (1025, 1003, 996, 983, 974, 956, 943, 930, 913, 889, 873, and 868 cm^{-1}) and Raman (1030, 1003, 996, 972, 948, 943, 890, and 876 cm^{-1}) spectra are observed. In this spectral range, the most intense IR band is observed at 1025 cm^{-1} and at 1003 cm^{-1} in the Raman spectrum.
[g]In the 830–720 cm^{-1} range, in both IR and Raman spectra, many weak bands are observed.
[h]In the 685–600 cm^{-1} range, a set of weak bands are observed in the IR spectrum. In the same spectral range, two well defined medium bands are observed in the Raman spectrum at 670 and 619 cm^{-1}. n.i., not investigated; n.o., not observed; n.a., not assigned. See Fig. 2 for atom labeling.

frequency peaks are predicted (model M.I) with quite high intensity (both ~523 km mol^{-1}), the peak at 1598 cm^{-1} with a medium intensity (131 km mol^{-1}) and the lower frequency peak with low intensity (4 km mol^{-1}). These modes are predicted by model M.III to be scattered over the 1653–1585 cm^{-1} range. In the experimental IR spectrum, the strong and quite broad band whose maximum is at ~1640 cm^{-1}, and those bands at ~1615 and 1565 cm^{-1} (band I) are then assigned to modes with significant contribution from the NH_2 bending coordinate.

Bands due to the ρNH_2 vibrations of the guanidinium group are predicted by model M.I to appear in the 1110–1025 cm^{-1} wavenumber range (M.II: 1153–1059 cm^{-1}; M.III: 1180–1075 cm^{-1}), with low IR (~1–10 km mol^{-1}) and Raman (~6–13 $Å^4$ amu^{-1}) intensities. According to theoretical predictions, the weak bands in the IR spectrum at 1109/1099 and 1074/1061 cm^{-1} and the Raman bands at 1109/1100 and 1062 cm^{-1} were then assigned to the rocking modes of the $–NH_2$ groups (band M).

2. Carboxylic ethyl ester moiety, –$COOCH_2CH_3$

All esters have strong characteristic IR bands due to the C=O and C–O–C asymmetric stretching vibrations.[26] For saturated aliphatic esters, the C=O stretching vibration absorbs at ~1750–1725 cm^{-1}, whereas the νC–O–C asymmetric and symmetric vibrations are usually observed around 1200 and 850 cm^{-1}, respectively.[27] In the IR spectrum of $BAEEH^+ \cdot Cl^-$, the C=O stretching vibration is observed at 1734 cm^{-1} (band G) and the bands due to the C–O–C asymmetric stretching vibrations at 1218 and 1200 cm^{-1} as strong bands (band L), while the less intense bands due to C–O–C symmetric stretching vibrations are observed at 855 and 843 cm^{-1}. All of these modes are observed in the Raman spectrum as medium to weak bands: 1736 cm^{-1} (νC=O; band G), 1220/1203 cm^{-1} (νC–O–C as; band L) and 855/846 cm^{-1} (νC–O–C s). The νC=O vibrational frequencies computed from models M.I and M.II are 1729 and 1724 cm^{-1}, respectively, whereas under model M.III the νC=O mode is split in four frequencies over the range 1670–1708 cm^{-1}.

3. Amide moiety, –C(=O)NH–

Formamide, H–C(=O)NH_2, is the simplest molecule containing an amide moiety. The structure and spectroscopic properties of formamide have been studied in inert gas matrices by Räsänen.[28,29] The interactions of formamide with hydrogen fluoride have been studied using matrix isolation spectroscopy and *ab initio* methods.[30] Since in the $BAEEH^+ \cdot Cl^-$ crystal the N–H is establishing intermolecular H-bond with the chloride anion, that study appeared relevant to shed some insight into the proposed vibrational assignments. Miyazawa[31] and Suzuki[32] studied the IR spectra of formamide in the liquid state, and Itoh *et al.*[33] in the crystalline state at various temperatures.

The modes involving the atoms of the OCN subunit show a great deal of mixing (this could be confirmed by visual inspection of the calculated vibrational modes, mainly in the case of solid-state simulations) since they incorporate framework atoms of nearly the same mass which are also involved in the additional π-conjugation (O=C–N $\leftrightarrow$ $^-$O–C=N^+). Very often, the absorptions in the CO and CN stretching regions are called amide I and amide III bands, respectively. The

amide I band can be described as an "asymmetric" stretch, while the amide III band can be described as the "symmetric" counterpart.[34] For simplicity, we are labeling amide I as νC=O and amide III as a mixture of νCN and δNH modes.

The amide group has an H-bond acceptor (C=O) and an H-bond donor (N–H). In fact, in the $BAEEH^+ \cdot Cl^-$ crystal both fragments of the amide group are involved in intermolecular H-bonds. A downward frequency shift is then expected for both C=O and N–H stretching frequencies when compared with isolated species. For example, the C=O stretching vibration of formamide isolated in an Ar matrix (free group) is observed at ~1745 cm^{-1}.[28] In the $BAEEH^+ \cdot Cl^-$ crystal, it is observed at ~1690 cm^{-1} (band H) in both IR and Raman spectra (being a very weak band in the Raman spectrum). The IR band due to the amide NH stretching vibration is observed in the $BAEEH^+ \cdot Cl^-$ crystal at ~3140 cm^{-1} (band D), and in isolated formamide at 3548/3427 cm^{-1}.[28] For the νC=O vibrational mode of the amide moiety, models M.I and M.II predict the frequencies of 1654 and 1650 cm^{-1}, respectively, while according to model M.III the frequencies should fall in the 1599–1590 cm^{-1} interval. For νNH model M.I predicts a feature at 3455 cm^{-1}, which is redshifted to 3388 cm^{-1} according to the model M.II and, in addition, split over the range 3244–3219 cm^{-1} in the case of the model M.III.

As expected, the normal mode analysis for $BAEEH^+$ shows that the CN stretching and the NH bending modes are strongly mixed. They are predicted to absorb at 1483 and 1460 cm^{-1} by model M.I (1522 and 1475 cm^{-1} by model M.II, and within the interval 1558–1530 cm^{-1} by model M.III), both bands being intense in IR spectrum. The group of bands around 1535 and 1490 cm^{-1} are then assigned to the CN stretching and NH bending modes (band K). These vibrations give rise to the weak Raman bands at 1540 and 1476 cm^{-1} (band K). In order to investigate the vibrational characteristics of CN bonds of different order, NCCN, ethylenediamine, and s-triazine derivatives have been investigated by Kordesch *et al.*[35] They found for the single, double and triple CN bond stretch frequencies ~1050, 1535, and 1900 cm^{-1}, respectively. Thus, one can say that the CN bond in $BAEEH^+ \cdot Cl^-$ crystal has a large degree of double bond character.

The band due to the amide N–H out-of-plane bending is predicted to appear at ~585 cm^{-1} with a medium IR intensity. This is a typical wavenumber for the bands due to the nonhydrogen-bonded N–H out-of-plane bending vibrations in secondary amides, RCONHR′.[36] In $BAEEH^+ \cdot Cl^-$ crystal, the N–H group is establishing an intermolecular H-bond with a chlorine ion, which makes the band to be broader and displaces it to higher wavenumbers. In fact, that calculated frequency is blue-shifted to 702 and 661 cm^{-1} in the case of the model M.II, and spread into the 862–832 cm^{-1} interval in model M.III (which sounds to be considerably overestimated, even taking into account that no scale factor was used for the simulation results from this model). The N–H out-of-plane bending vibration is here tentatively assigned to the quite broad IR band centered at 708 cm^{-1}.

IV. CONCLUSION

Crystalline $BAEEH^+ \cdot Cl^-$, an appropriate PEAs' model compound, was studied by an integrated experimental and theoretical approach.

Single crystals of $BAEEH^+ \cdot Cl^-$ were obtained and their structure was solved by x-ray technique. The $BAEEH^+ \cdot Cl^-$ crystal was found to be monoclinic, space group $P2_1$. Two symmetry independent cations, with different conformations, were found in the unit cell.

The theoretical structural parameters (bond lengths and valence angles) were predicted by using three distinct models (*in vacuo* and solid-state) and it was found an overall remarkable agreement among these structural parameters as predicted by the developed models and between these and the experimental data. Thus, in the case of the title compound, even the simplest model can predict fairly well most of the structural features.

The structural information was then used in the interpretation of the IR and Raman spectra of the substance. The assignment of the spectra of $BAEEH^+ \cdot Cl^-$ was supported by the theoretical calculations and helped by comparison with spectra of similar compounds.

ACKNOWLEDGMENTS

A. C. Fonseca acknowledges "Fundação para a Ciência e Tecnologia," Grant: SFRH/BD/41305/2007. S. Jarmelo acknowledges "Fundação para a Ciência e a Tecnologia," Portugal, for the Grant SFRH/BPD/22410/2005. Project FCT-PTDC/QUI/71203/2006, also supported by COMPETE and FEDER.

[1] M. T. Casas, S. Gesti, and J. Puiggali, Cryst. Growth Des. **5**(3), 1099 (2005).
[2] E. Botines, M. T. Casas, and J. Puiggali, J. Polym. Sci., Part B: Polym. Phys. **45**(7), 815 (2007).
[3] Y. K. Feng and J. T. Guo, Int. J. Mol. Sci. **10**(2), 589 (2009).
[4] J. Montane, E. Armelin, L. Asin, A. Rodriguez-Galan, and J. Puiggali, J. Appl. Polym. Sci. **85**(9), 1815 (2002); S. I. Han, B. S. Kim, S. W. Kang, H. Shirai, and S. S. Im, Biomaterials **24**(20), 3453 (2003); J. Puiggali and J. A. Subirana, J. Pept. Sci. **11**(5), 247 (2005).
[5] M. T. Casas and J. Puiggali, J. Polym. Sci. Part B: Polym. Phys. **47**(2), 194 (2009).
[6] N. Paredes, M. T. Casas, J. Puiggali, and B. Lotz, J. Polym. Sci. Part B: Polym. Phys. **37**(17), 2521 (1999).
[7] A. C. Fonseca, S. Jarmelo, R. A. Carvalho, R. Fausto, M. H. Gil, and P. N. Simoes, J. Phys. Chem. B **114**(18), 6156 (2010).
[8] J. Lipkowski and K. Suwińska, in *Practical Aspects of Computational Chemistry*, edited by J. Leszczynski and M. K. Shukla (Springer, Netherlands, 2010), pp. 241.
[9] G. M. Sheldrick, *SHELXS97 & SHELXL97*, University of Göttingen: Göttingen, Germany, 1997.
[10] H. D. Flack, Acta Crystallogr., Sect. A: Found. Crystallogr. **39**, 876 (1983).
[11] M. J. Frisch, G. W. Trucks, H. B. Schlegel *et al.*, GAUSSIAN 03, Revision D.01, Gaussian, Inc, Wallingford, CT, 2004.
[12] R. Parr and W. Wang, *Density-Functional Theory of Atoms and Molecules*. (Oxford University Press, New York, 1994); R. Neumann, R. H. Nobes, and N. C. Handy, Mol. Phys. **87**(1), 1 (1996).
[13] A. D. Becke, Phys. Rev. A **38**(6), 3098 (1988); C. T. Lee, W. T. Yang, and R. G. Parr, Phys. Rev. B **37**(2), 785 (1988).
[14] A. D. Becke, J. Chem. Phys. **98**(7), 5648 (1993).
[15] C. Y. Peng, P. Y. Ayala, H. B. Schlegel, and M. J. Frisch, J. Comp. Chem. **17**(1), 49 (1996).

[16]J. Hutter *et al.*, Computer code CPMD (Copyright IBM Corp. and MPI-FKF Stuttgart).
[17]S. Goedecker, M. Teter, and J. Hutter, Phys. Rev. B **54**(3), 1703 (1996); C. Hartwigsen, S. Goedecker, and J. Hutter, Phys. Rev. B **58**(7), 3641 (1998).
[18]See supplementary material at http://dx.doi.org/10.1063/1.3565966 for tables of computed geometrical parameters, IR and Raman data, and figures of optimized structures and comparison between calculated and experimental geometrical parameters.
[19]W. Koch and M. C. Holthausen, *A Chemist's Guide to Density Functional Theory*, 2nd ed. (Wiley VCH, Berlin, 2001).
[20]S. Jarmelo, I. Reva, M. Rozenberg, M. R. Silva, A. M. M. Beja, and R. Fausto, J. Phys. Chem. B **112**(27), 8032 (2008); S. Jarmelo, P. R. Carey, and R. Fausto, Vib. Spectrosc. **43**(1), 104 (2007); S. Jarmelo, I. Reva, P. R. Carey, and R. Fausto, Vib. Spectrosc. **43**(2), 395 (2007); S. Jarmelo, I. Reva, M. Rozenberg, P. R. Carey, and R. Fausto, Vib. Spectrosc. **41**(1), 73 (2006).
[21]I. M. Walker and P. J. McCarthy, Inorg. Chem. **31**(20), 4122 (1992).
[22]M. Drozd and J. Baran, Spectrochim. Acta, Part A **61**(13–14), 2953 (2005).
[23]M. Drozd, J. Baran, and A. Pietraszko, Spectrochim. Acta, Part A **61**(13–14), 2809 (2005).
[24]M. Drozd and J. Baran, Spectrochim. Acta, Part A **64**(4), 867 (2006).
[25]W. J. Jones, Trans. Faraday Soc. **55**(4), 524 (1959).
[26]L. J. Bellamy, *The Infrared Spectra of Complex Molecules* (Chapman & Hall, London, 1975).
[27]I. I. Maes, W. A. Herrebout, and B. J. Vanderveken, J. Raman Spectrosc. **25**(7–8), 679 (1994).
[28]M. Rasanen, J. Mol. Struct. **101**(3–4), 275 (1983).
[29]M. Rasanen, J. Mol. Struct. **102**(3–4), 235 (1983).
[30]R. B. Bohn and L. Andrews, J. Phys. Chem. **93**(15), 5684 (1989).
[31]S. Mizushima and T. Shimanouchi, Annu. Rev. Phys. Chem. **7**, 445 (1956), and references therein.
[32]I. Suzuki, Bull. Chem. Soc. Jpn. **33**(10), 1359 (1960).
[33]K. Itoh and T. Shimanou, J. Mol. Spectrosc. **42**(1), 86 (1972).
[34]A. G. Walton, *Polypeptides and Protein Structure* (Elsevier North Holland, New York, 1981).
[35]M. E. Kordesch, W. Stenzel, and H. Conrad, Surf. Sci. Lett. **186**(3), 601 (1987).
[36]M. S. Rozenberg, J. Appl. Spectrosc. **23**, 1353 (1975).